Chemical Engineering Journal 445 (2022) 136690

Contents lists available at ScienceDirect

Chemical Engineering Journal

journal homepage: www.elsevier.com/locate/cej

The scale-up of electrochemically mediated atom transfer radical polymerization without deoxygenation

Francesco De Bon [a], Rita G. Fonseca [a], Francesca Lorandi [b,c], Arménio C. Serra [a], Abdirisak A. Isse [b], Krzysztof Matyjaszewski [c], Jorge F.J. Coelho [a,*]

[a] University of Coimbra, Centre for Mechanical Engineering, Materials and Processes, Department of Chemical Engineering, Rua Sílvio Lima, Pólo II, 3030-790 Coimbra, Portugal

[b] Department of Chemical Sciences, University of Padova, Via Marzolo 1, 35131 Padova, Italy

[c] Department of Chemistry, Carnegie Mellon University, 4400 Fifth Ave, 15213, Pittsburgh, PA, USA

ARTICLE INFO

Keywords:
Scale-up
Electrochemistry
ATRP
Polymers
Oxygen
Pyruvate

ABSTRACT

The scale-up of Atom Transfer Radical Polymerization (ATRP) from 15 mL to 15 L (scale-up factor 1000) by galvanostatic simplified electrochemically mediated ATRP (*se*ATRP) is disclosed. An electrochemical O_2 scavenging cycle was embedded in the ATRP equilibrium to allow self-degassing of the mixture and avoid impractical deoxygenation procedures. Low volume *se*ATRP of acrylamide in water was optimized by studying various reaction parameters, including the concentrations of scavenger, supporting electrolyte, type of initiator and ligand, and catalyst loading. The target reaction was scaled up from 0.015 L to 15 L. At all volumes and up to 15 L, polymerizations were relatively fast and produced well-defined polyacrylamide with narrow molecular weight (MW) distributions. All reactions were powered by renewable electricity, obtained from a photovoltaic plant. Several water-soluble monomers, including (meth)acrylic acid and methacrylamide, were polymerized at pH ranging from 1.0 to 7.4, without compromising the self-degassing mechanism. These results show a feasible scale-up of *se*ATRP and could foster its adoption by polymer industries promoting a more widespread use of controlled radical polymerizations.

1. Introduction

The goal of chemists in scaling-up reactions is to unequivocally demonstrate that large batches of a desired product are obtained without compromising product quality and yield [1]. To scale-up a process from a laboratory reactor to an industrial one, chemists have several options: continuous lab-scale operation, numbering-up, and scale-up. The last is usually chosen because it is most likely to yield an acceptable result, when throughput and capital costs are considered [1]. In electrochemical engineering and large electrochemical production plants, numbering-up (parallel mode) is also often employed [2]. In addition, design and full understanding of the reaction are important to identify problems and solutions along the scale-up development, not just for fundamental understanding. Polymerizations, like any other chemical process, obey these guidelines.

Atom Transfer Radical Polymerization (ATRP) is a widely used Reversible Deactivation Radical Polymerization (RDRP) technique that provides scientists in various branches of chemistry, materials and life sciences the ability to design well-defined, and often complex polymeric structures. ATRP is a catalytic process mediated by Cu(I)/Cu(II) based complexes and is tolerant to a variety of functional groups and solvents. Very active copper catalysts with strongly negative reduction potentials enabled well-controlled polymerizations at catalyst loadings as low as 10–100 parts per million (ppm, relative to the monomer concentration), in H_2O and organic solvents [3,4]. $[Cu^{I}L]^{+}$ (L = ligand, typically *N*-polydentate amine) activates the dormant C–X (X = Br, Cl) polymer chain end, forming $[X\text{-}Cu^{II}L]^{+}$ and a carbon-centered radical. The $[X\text{-}Cu^{II}L]^{+}$ complex deactivates the radical after a few propagation events, regenerating a dormant species. Because ATRP is a radical polymerization, it is inhibited by O_2 in the vessel and by continuous diffusion of the gas in the mixture if it is open to air. Indeed, O_2 can react with the propagating radicals and terminate the polymerization. [5–10]. In addition, even trace amounts of O_2 can inhibit polymerization by rapid oxidation of the $[Cu^{I}L]^{+}$ activator [11]. Therefore, if O_2 is not removed from the mixture, both radicals and Cu^{I} species can rapidly react with it to form peroxyl radicals and hydroperoxo complexes or other Cu^{II}

* Corresponding author.
E-mail address: jcoelho@eq.uc.pt (J.F.J. Coelho).

https://doi.org/10.1016/j.cej.2022.136690
Received 14 March 2022; Received in revised form 19 April 2022; Accepted 26 April 2022
Available online 30 April 2022

complexes (Scheme 1) [12,13].

Reactions of alkyl radicals with O_2 have rate constants close to the diffusion-controlled limit [14,15]. However, since the concentration of $[Cu^IL]^+$ is 10^3 to $> 10^6$ times higher than that of the propagating radicals, the dominating reaction of O_2 in solution is oxidation of the activator $[Cu^IL]^+$ to $[HOO\text{-}Cu^{II}L]^+$. If the hydroperoxo complex can be converted back to $[Cu^IL]^+$ through a reductive pathway involving chemical or electrochemical reduction, O_2 can be chemically washed out of the mixture (Scheme 1). Because of its high sensitivity to O_2, ATRP requires often special equipment and deoxygenation by injecting an inert gas prior to the polymerization, which can be cumbersome and costly, especially on a large scale reaction [16,17]. A few years after the introduction of ATRP, well-controlled ATRP in the presence of a limited amount of O_2 was obtained by using Cu^0 as a reducing agent [18]. This concept was later extended to ATRP using copper wires [19–21] or plates [22–26] and other reducing agents, such as sodium dithionite [27], Fe^0 [28–31], Zn^0 [32], ascorbic acid [33,34], tin(II) 2-ethylhexanoate [35], and tertiary amines. [36] A few ATRP systems based on enzymatic degassing [29,37] were carried out in completely open reaction vessels with continuous O_2 diffusion. [38] Achieving therefore oxygen tolerance is indeed of academic importance but even more for industrial-like large scale reactions [29,39–56]. In 2020, photoinduced initiators for continuous activator regeneration (PICAR) ATRP enabled regeneration of $[Cu^IL]^+$ by excitation of $[X\text{-}Cu^{II}L]^+$, followed by one electron donation from the excess amine ligand, with simultaneous removal of dissolved O_2 in the presence of sodium pyruvate. PICAR ATRP was effective even under continuous diffusion of O_2 from the atmosphere into the mixture and no stirring, in contrast to previous ATRPs carried out in sealed vessels with a limited amount of O_2 in the reaction mixture or based on enzymatic degassing. It should be noted however that open vessels may not be the preferred type of industrial reactors and are not suitable for gaseous or volatile monomers, which besides often having an acrid odor, can be toxic or carcinogenic. Among all externally controlled ATRP methods, electrochemically mediated ATRP (*e*ATRP), introduced in 2011 [57], is experiencing its heyday [57–63]. The concept behind *e*ATRP is that the ratio of activator to deactivator is tightly controlled by an electrochemical redox process occurring at an electrode surface [46–48]. Factors such as applied current (I_{app}), applied potential (E_{app}), or even the total charge passed (Q) can be fixed *a priori* in *e*ATRP, to constrain the redox equilibrium, and thus precisely control the polymerization. *e*ATRP is also redox-switchable, as it can be stopped and (re)initiated (ON/OFF toggle) by modulating the electrochemical stimulus or even by switching off the cell, achieving temporal control over the process. *e*ATRP provided very positive results in the synthesis of well-defined architectures, becoming increasingly attractive for scale-up in recent years. Although some limitations remain, particularly linked to its elaborate reaction setup, *e*ATRP has become more user-friendly. Typically, *e*ATRP is performed using a three-electrode system under potentiostatic conditions (fixed E_{app}). However, several modifications have improved and redesigned the setup, including: 1) the use of a sacrificial counter electrode (CE), which is introduced directly into the reaction mixture in the so-called simplified *e*ATRP (*se*ATRP);[64] 2) galvanostatic conditions, i.e. constant current electrolysis, without the need for a reference electrode;[62,65] and 3) the use of working electrodes made of materials less expensive than the usually employed Pt (e.g., SS304), with little or no effect on the polymerization outcome [66,67]. The most likely scenario for the scale-up of *e*ATRP is a closed reactor [68–70] with O_2 diffusing from the confined headspace into the reaction mixture, if not removed physically or chemically. To promote the scale-up of *e*ATRP and reduce the challenges associated to ATRP on an industrial scale, we have embedded an electrochemical O_2 scrubbing cycle into the ATRP equilibrium, mediated by the ATRP catalyst itself. Inspired by PICAR ATRP [12], the process proposed herein avoids the need of enzymes, while employing electricity from renewable resources as a driving force. Non-enzymatic degassing is highly beneficial and significantly improves O_2 removal from large mixtures, allowing for a fully functional, effective, and more user-friendly scale-up. With a scale-up factor of 1000, we successfully scaled up from 15 mL to 15 L the first self-degassing, large-volume, galvanostatic *e*ATRP in H_2O. High monomer conversions were reached in a relatively short time, demonstrating a true scale-up of *e*ATRP. The polymerization at 15 L is likely one of the largest-volume ATRP ever reported, and the largest-volume *e*ATRP reported in the literature.

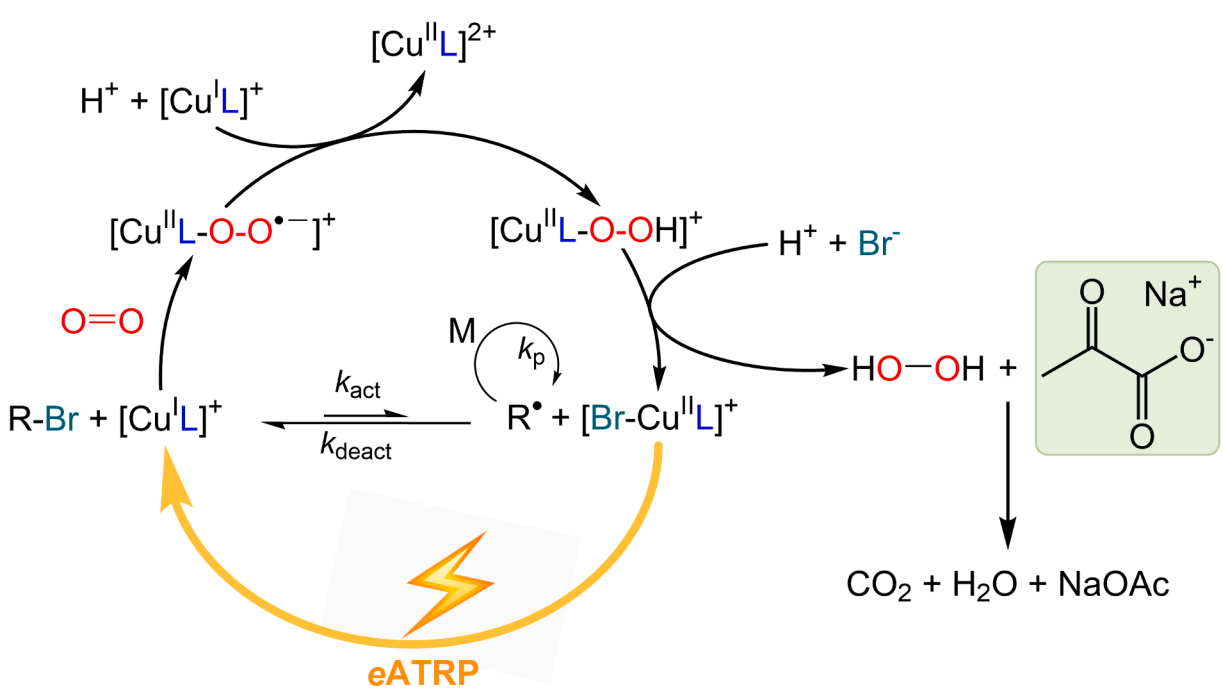

Scheme 1. Proposed mechanism of *e*ATRP with embedded O_2 scavenging cycle for self-degassing. M is the monomer, while k_{act}, k_{deact} and k_p are the activation, deactivation and propagation rate constants, respectively.

2. Results and discussion

2.1. Target reaction for scale-up.

There are numerous aspects to consider for scaling up a polymerization: reaction mechanism, reactor configuration and operating conditions, heat removal, fluid dynamics, mass transfer, thermodynamics, boundary conditions, process dynamics and system stability [1,71]. In addition, an electrochemical scale-up presents other challenges, such as electrode and reactor fabrication, current/potential ratios, membrane/separator materials, charge transfer and electric field distribution [71]; typically predictions/modeling are extensively evaluated before the implementation [72]. These aspects are critical on a large scale, but it is essential that the target reaction is thoroughly investigated and understood prior to scale-up (Scheme 2).

An ATRP is influenced by several components, namely, solvent, monomer, ligand, catalyst type and structure, type of supporting electrolyte (only for *e*ATRP), initiator, polymerization medium (homogeneous or heterogeneous), and type of driving force [58,73,74]. In such a multifaceted scenario, cost-efficiency becomes the fundamental aspect [75,76]. The scale-up requires to identify a polymerization that is economic not only at laboratory scale but also at large scale. Each component of the ATRP system was critically evaluated to find the most reasonable and cost-effective balance between cost and reaction outcome (see **Supporting Information, Sections S3 and S5**). The target reaction was selected to be an aqueous polymerization: H_2O is a clean, universally available, inexpensive, and renewable solvent. Aqueous *e*ATRP is very attractive from both economic and environmental points of view. In recent years, water-soluble poly(meth)acrylates and polyacrylamides have been successfully prepared using *e*ATRP forming polymers with relatively narrow dispersity ($Đ$) and experimental molecular weight values (M_n) close to theoretical values [62,77,78]. However, aqueous *e*ATRP presents some challenges. The Cu-X bond in the $[X\text{-}Cu^{II}L]^+$ deactivator can easily dissociate in H_2O due to low halidophilicity of Cu^{II} (i.e. binding constants for X^- to $[Cu^{II}L]^{2+} \leq 10$ M^{-1}) [78]. Therefore, either high catalyst concentrations or the addition of halide salts are required [77,79]. The addition of excess X^- by introducing a salt that can also act as supporting electrolyte, promotes the formation of $[X\text{-}Cu^{II}L]^+$ and significantly improves polymerization control. Moreover, temperature has an important effect on aqueous ATRP. The nucleophilic substitution (solvolysis) of alkyl halides in H_2O is suppressed at low temperatures. Therefore, aqueous *e*ATRPs carried out at relatively low temperature (<70 °C) and Cu catalyst loading < 500 ppm were most effective for some water-soluble monomers [80–82]. The ideal monomer for scale-up should be hydrophilic, should have a high propagation rate constant (k_p), polymerize near room temperature, be solid or liquid at the desired temperature; it must also be inexpensive and commercially available, preferably without inhibitor, industrially relevant, and made from inexpensive starting materials. Acrylamide (AAm) is a monomer that meets these requirements. Moreover, PAAm has a broad market, and very high monomer conversion is usually reached at the laboratory scale [81,83–90], which minimizes intensive post-processing of the mixture. ATRP of acrylamides is known and the literature provides proper starting conditions for further optimization [80–82]. The best catalyst for acrylamides is a Cu complex with tris(2-dimethylaminoethyl)amine (Me_6TREN) as ligand, while 2-hydroxyethyl 2-bromoisobutyrate (HEBiB) is typically used as initiator in aqueous polymerizations. Although both Me_6TREN and HEBiB are commercially available, they can be easily prepared in high yields and their on-site synthesis is by far less expensive than the commercial purchase. In *e*ATRP, a supporting electrolyte is necessary to make the solution electrically conductive, therefore inexpensive NaBr was chosen, which also acted as a halide source. Sodium pyruvate (SP), prepared from pyruvic acid and sodium hydroxide, [91] has been successfully used as reactive oxygen species (ROS) scrubber in PICAR ATRP of *N*-isopropylacrylamide (NIPAAm) and methyl acrylate (MA) [12]. SP was used also in this study. The chemistry of SP is well-understood in H_2O and even in the atmosphere [12,92–96], and it does not pose any threat to ATRP activation or deactivation. Regarding the cell setup, low-cost electrode materials should be used [64–67,97,98], therefore reactors made of stainless steel (SS) SS304, acting also as the cathode, were employed together with sacrificial aluminum anodes, thus working in a *se*ATRP setup. Beside the electrodes, the power source becomes crucial for large-volume reactions. We used renewable electric energy obtained from sunlight by a photovoltaic system installed on the roof of the Chemical Engineering Department. This choice permits a cleaner *e*ATRP; in addition, AAm can be provided as bio-acrylamide, as some chemical industries already reached a bio-synthesis of this monomer rather than relying on oil-based feedstocks [99]. Four reactors were used in the successive phases of the scale-up: a traditional five-neck glass cell, a 50 mL SS304 compact reactor for the primary optimization, followed by a 2 L, and 18 L SS304 electrochemical reactors (Fig. 1).

2.2. Primary optimization.

The primary optimization of self-degassing *se*ATRP involves numerous challenges: 1) embedding an O_2 washing pathway into the *e*ATRP equilibrium; 2) raising the reaction temperature to values above the typical value (0 °C) used for ATRP of acrylamides, [81–83] without triggering parasitic reactions [83,100]; 3) minimizing reagent loadings, and thus energy requirements, without compromising the kinetics, 4) defining a robust electrochemical scale-up protocol for larger reactors,

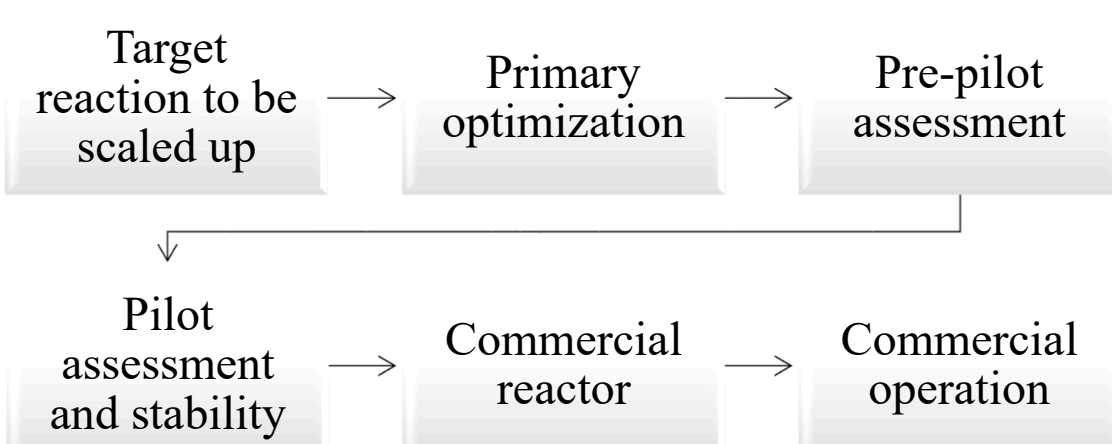

Scheme 2. Proposed flowchart for *e*ATRP scale-up, from targeting the reaction to scale to considering the requirements of a possible future commercial process.

Fig. 1. Digital pictures of a) 50 mL, b) 2 L and c) 18 L reactors; heads of the (d) 2 L and (e) 18 L reactors; f) the 18 L reactor loaded with the polymerization mixture for the 15 L *se*ATRP of AAm (see Table 3 entry 6).

5) dealing with magnetic stirring for reaction volumes beyond 5.0 L, without dramatic changes in mass transfer, and 6) dealing with limitations of the electrochemical equipment if high current outputs are required. First, we investigated the stability of the catalyst in the presence of sodium pyruvate, NaBr or NaCl, and the effect of the scavenger on the activation and deactivation rate constants, k_{act} and k_{deact}, respectively, and the ATRP equilibrium constant, K_{ATRP}. 2-Bromopropionamide (BrPAm) or 2-chloropropionamide (ClPAm) were used as model chain-ends for PAAm (**Section S4**). Cyclic voltammetry of $[Cu^{II}Me_6TREN]^{2+}$ in H_2O/AAm (10 wt%) showed a quasi-reversible peak couple, which did not vary upon addition of excess X^- (**Figure S5**), indicating low halidophilicity of the Cu complex in aqueous media. Addition of a large excess of sodium pyruvate did not substantially change the voltammetric response, while remarkable catalytic enhancement of the cathodic peak was observed when HEBiB was added (**Figures S7-S8**). The cathodic current enhancement is due to Cu(I)-catalysed activation of the initiator, which otherwise cannot generate radicals by direct reduction at the electrode at the chosen potential window. Electrode reduction of HEBiB requires potentials significantly more negative than the standard redox potential (E°) of the copper catalyst [101]. A rotating disk electrode (RDE) [102] was used to measure the values of k_{act} of BrPAm and ClPAm by $[Cu^{I}Me_6TREN]^+$, yielding 1206 $M^{-1}s^{-1}$ and 8.4 $M^{-1}s^{-1}$, respectively. Thus, the activation of Br-capped PAAm chains was relatively fast, and over two orders of magnitude more rapid than for Cl-capped chains, in agreement with previous reports [78]. The addition of a large excess (100 equiv.) of NaBr or NaCl caused minimal variation in the activation kinetics, further suggesting that the catalyst has low halidophilicity. Further addition of

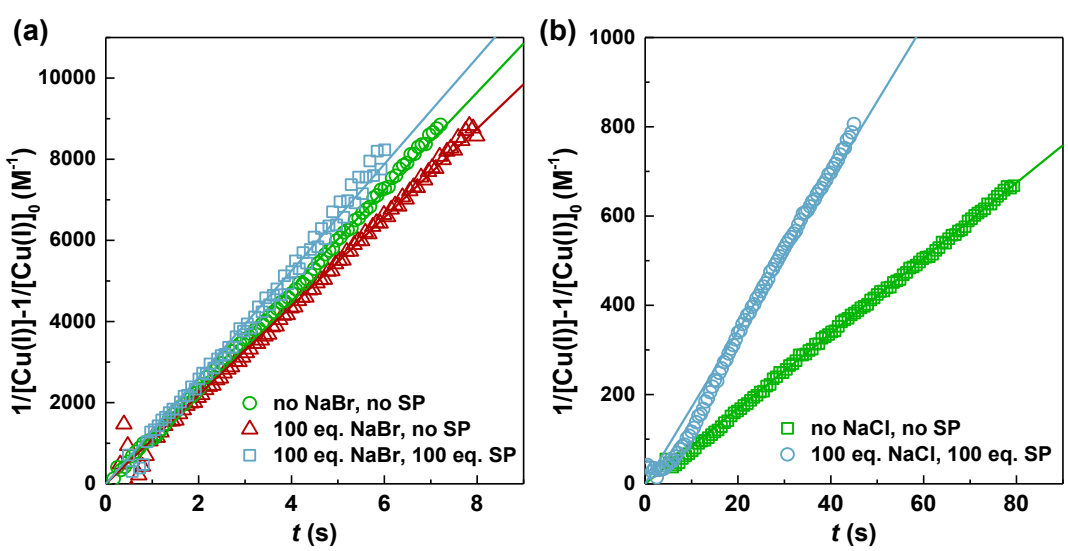

Fig. 2. Kinetic analysis of BrPAm (a) and ClPAm (b) activation by $[Cu^{I}Me_6TREN]^+$ in H_2O/AAm (10 wt%) in the absence and presence of 100 equiv. NaX and/or sodium pyruvate (SP), measured using a rotating disk electrode (RDE), at E_{app} = 0.15 V vs SCE, and rotation speed = 4000 rpm.

sodium pyruvate in equimolar amount to the NaX salt increased the observed rate constants by a factor of 1.2 and 2 for BrPAm and ClPAm, respectively (Fig. 2). Pyruvate anion is capable of binding to Cu complexes, however it has only a small effect on the kinetics in the studied mixtures. The value of K_{ATRP} for the system composed of $[Cu^{I}Me_6TREN]^+$ and ClPAm was also measured by RDE [103], giving $K_{ATRP} = 5.1 \times 10^{-6}$. In the presence of excess of both sodium pyruvate and NaCl, the observed K_{ATRP} was ~ 3 times smaller (1.6×10^{-6}). As a result, k_{deact} (calculated as k_{act}/K_{ATRP}) increased by about 1 order of magnitude in the presence of sodium pyruvate, which can result in more effective deactivation of propagating radicals, and thus better control. The equilibrium constant for the BrPAm-based system was above the upper limit of the RDE method; however one can expect a K_{ATRP} value on the order of 10^{-5}, and thus $k_{deact} \sim 10^8\ M^{-1}s^{-1}$ [104]. Overall, the use of Br^- ions and C-Br chain end should result in faster and better controlled polymerization, compared to Cl^- and C-Cl chain end, as is typically observed in ATRP.

After the voltammetric study, the polymerization was investigated in detail in an undivided glass cell, with a Pt gauze as cathode and an Al wire as a sacrificial anode, at a total volume $V = 15$ mL (**Tables 1 and S6**).

This allowed to fully understand the polymerization behavior and to identify the reagents that can be used in smaller amounts, in view of employing larger reactors. The polymerization was investigated in detail by changing the concentrations of SP and NaBr (or NaCl), degree of polymerization, catalyst load, and "type" of H_2O and electrolyte (NaBr or NaCl). Also, the effect of using a buffer was examined. Polymerizations with NaBr were more controlled than those with NaCl, in terms of optimal electrolyte amount, $Đ$ of PAAm and charge consumption. In addition, raising the temperature to $T = 10$ °C did not affect control and conversion. We also found that using 0.05 M SP + 0.05 M NaBr gave the same outcome as when 0.1 M concentration of both was used. The catalyst concentration was diminished to 5×10^{-4} M. Electrogenerated H_2O_2 should be<0.05 M but this is a very high amount. Typical dissolved O_2 concentrations are below 0.2–0.3 mM if the solution is exposed to open-air, so the maximum amount of electrogenerated H_2O_2 depends on the maximum amount of dissolved O_2, which is low, considering that we operate in a closed system with purged headspace. Further results are shown in **Tables S6-S7**. This preliminary set of experiments suggested the selection of the optimal conditions reported in Table 2.

Once the best laboratory-scale mixture composition was identified, the polymerization was attempted by galvanostatic *se*ATRP (Fig. 3) [65]. Galvanostatic electrolysis with one value of applied current or multistep currents is the usual choice for large scale electrosynthesis [105,106]. The choice of the applied current (I_{app}) and step length must consider various issues and parameters, including catalyst concentration, overall required charge, electrode surface area (S) and surface/volume ratio (S/V). This is an unexplored area, lacking literature details, therefore we had to identify proper adjustment factors when needed (Table S8). Potentiostatic *se*ATRP was employed to understand the effect of mixture composition, reactor, and electrodes parameters. After careful and extensive screening of polymerization conditions by potentiostatic *se*ATRP (Table 1 and **Table S6**), a candidate polymerization was chosen for the scale-up (Table 1, **entry 5** and Fig. 3). The reaction conditions summarized in Table 2 were used to compare a potentiostatic *se*ATRP in a glass cell (solution volume = 15 mL) with a Pt working electrode (Fig. 3, black squares) with a galvanostatic *se*ATRP in a compact 50 mL SS304 reactor ($V = 40$ mL, geometric surface area of the cathode exposed to the solution, $S = 53\ cm^2$) (Fig. 3, red circles). Both reactions were fast and very well-controlled, reaching ~ 90% conversion within 2 h (Fig. 3 **a,b**). Polymers with narrow monomodal molecular weight distributions were obtained, shifting toward higher molecular weight as conversion increased (Fig. 3 **c,d**). A short induction

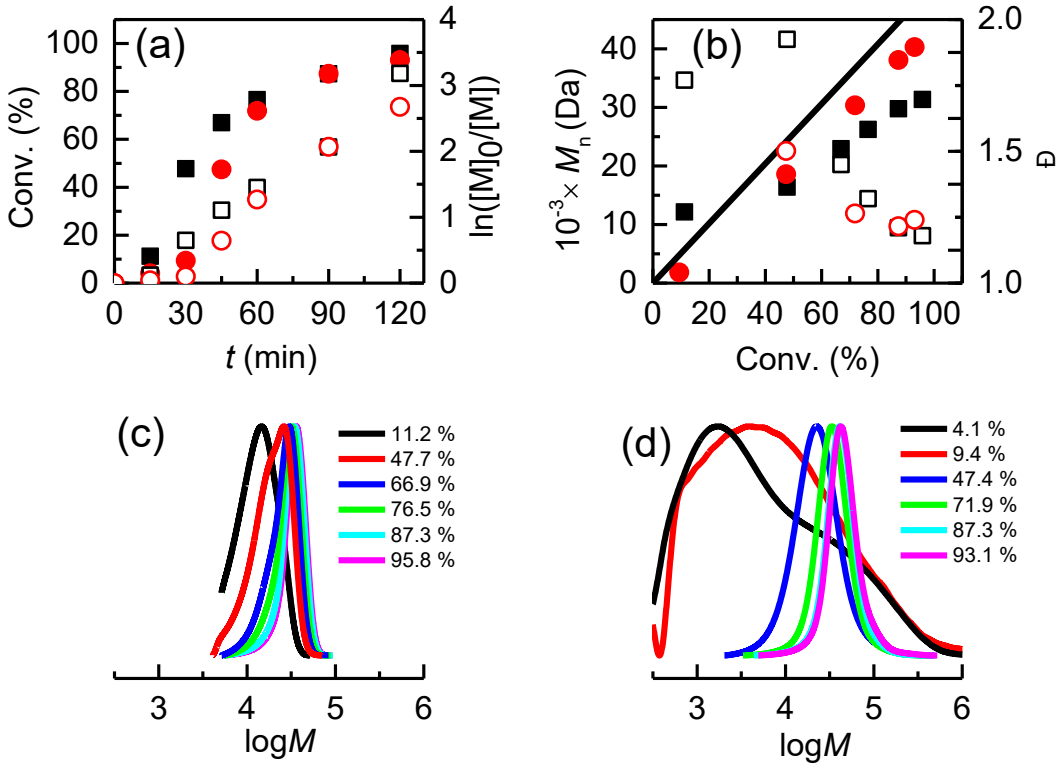

Fig. 3. 15 mL-potentiostatic *se*ATRP with Pt electrode (■ black) vs 40 mL-galvanostatic *se*ATRP with stainless steel 304 reactor scaffold (● red) of AAm in H_2O at 10 °C: a) evolution of conversion (filled symbols) and $\ln([M]_0/[M])$ (empty symbols) vs time; b) evolution of M_n^{GPC} (filled symbols) and $Đ$ (empty symbols) vs conversion; c, d) normalized evolution of molecular weight distribution of PAAm from potentiostatic (c) and galvanostatic (d) *se*ATRPs. In galvanostatic *se*ATRP (d), bimodality in the first two chromatograms at conv. = 4.1 and 9.4% is caused by normalization.

Table 1
Results of 15 mL *se*ATRP of AAm (10 wt%) in the presence of NaBr and SP.[a].

Entry	NaBr (M)	$CuBr_2$ (mM)	E_{app}	SP (M)	t (h)	Conv. (%)[b]	$10^{-3} \times M_n$ [c]	$10^{-3} \times M_n^{th}$ [d]	$Đ$ [e]		Observations
1	0.1	1	E_{pc}	0.1	3	–	–	–	–	3.77	Steady-state O_2 diffusion, no observed polymerization
2	0.1	1	E_{pc}	0.1	1.5	97	43.0	48.3	1.20	1.37	Blanketing at $t = 0$
3	0.1	1	E_{pc}	0.1	1.5	94	41.1	43.3	1.21	1.08	No buffer
4	0.1	0.5	E_{pc}	0.1	2	87	45.0	43.9	1.17	1.42	Buffer
5	0.05	0.5	E_{pc}	0.05	1.5	93	40.4	46.9	1.18	1.46	Buffer, $T = 10$ °C
6	0.05	0.5	I_{app}	0.05	2.5	93	40.3	46.8	1.24	8.17	Buffer, $T = 10$ °C, $V = 40$ mL

[a] Conditions: [AAm]/[HEBiB]/[$CuBr_2$]/[Me_6TREN] = 704/1/x/2, where x = 1 or 0.5, according to the third column, DP = 704. WE = Pt mesh approx. 6 cm^2, CE = aluminum wire directly immersed into the working solution. Stirring = 700 rpm. E_{pc} = cathodic peak potential. [b] Calculated from ^{1}H NMR in D_2O + 2 vol% DMF as internal standard. [c] Calculated from aqueous GPC with 6 narrow poly(sodium methacrylate) standards at $T = 35$ °C. [d] Calculated from ^{1}H NMR: M_n^{th} = Conv. × DP × MW_{AAm} + MW_{HEBiB}. [e] $Đ = M_w/M_n$. Additional comments: entries 1–4, 6: 0.012 M phosphate buffer and variable blanketing; entry 5: no buffer added and blanketing before electrolysis; entry 6: V_{TOT} = 40 mL in the compact 50 mL SS304 reactor with Al sacrificial anode.

Table 2
Chemical composition of the polymerization mixture of AAm.

Name	Empirical Formula	Role	Concentration
AAm	C_3H_5NO	Monomer	1.41 M
H_2O	H_2O	Solvent	~50 M
Copper(II) Bromide	$CuBr_2$	Pre-catalyst	5×10^{-4} M
Tris(2-dimethylaminoethyl) amine	$C_{12}H_{30}N_4$	Ligand	2×10^{-3} M
Sodium Bromide	NaBr	Supporting electrolyte	5.0×10^{-2} M
Sodium Pyruvate	$C_3H_3O_3Na$	ROS scrubber	5.0×10^{-2} M
Sodium dihydrogenphosphate	NaH_2PO_4	Buffer component	1×10^{-2} M
Potassium hydrogenphosphate	K_2HPO_4	Buffer component	1.8×10^{-3} M
2-Hydroxyethyl 2-bromoisobutyrate	$C_6H_{11}BrO_3$	Alkyl halide Initiator	2.0×10^{-3} M
Dimethylformamide	C_3H_7NO	Internal standard	2.6×10^{-4} M (2 vol%)

period (15–30 min) was observed for galvanostatic *se*ATRP (Fig. 3**a**). This is likely due to two separate processes. The first process is a self-cleaning of the stainless-steel surface, as some charge is used to modify the oxide layer that is present on the stainless-steel surface. The second process is the oxygen consumption which takes place once oxide-free electrode surface becomes available to reduce the catalyst from Cu(II)/L to Cu(I)/L. It is also possible that these two processes occur concurrently. Thus, the short induction period is attributed to the contributions of these two processes, which both result in charge consumption prior to the onset of the polymerization. After these encouraging results, the candidate mixture (Table 2) was adopted for the scale-up.

2.3. Large volume seATRP.

The combination of all above mentioned variables defines an applied current value that allows the polymerization to proceed at virtually any volume. Another requirement for successful large-scale electrolysis is efficient mass and charge transfer. As the solution is highly electrically conductive, we decided to rely on magnetic agitation for mass transfer. We employed a 7.5 cm diameter hub-shaped AlNiCo magnet, which provided sufficient stirring up to 15 L. The hub shape is preferred to a cylindrical one because it allows higher turbulence at lower torques, without stirrer uncoupling from the magnet. We found during the experimental design that *se*ATRP of 10 L and 15 L required currents greater than the maximum output (±0.8 A) of our potentiostat/galvanostat. In addition, a first attempt at 5 L showed some limitations of mass transfer that caused a runaway of the reaction at high current output ($|I_{app}|$ = 0.545 mA) and led to passivation of the reactor surface. To circumvent these limits, we decided to maintain $|I_{app}|$ below 300 mA. Applying a lower I_{app} resulted in a slower $[Cu^IL]^+$ regeneration, and thus a slower O_2 consumption at the beginning of the reaction, which delayed the onset of polymerization (up to 3 h induction period was observed at V = 15 L). The electrolysis programs are shown in **Table S9** and **Figure S13**. Using the reaction conditions reported in Table 2, scale-up of *se*ATRP of AAm was evaluated at 0.5, 1.0, 5.0, 10.0 and 15.0 L (Table 3, **entries 1–6**).

First-order kinetic plots and molecular weight evolutions vs conversion are shown in Fig. 4.

The correct electrolysis programs afforded reactions that were relatively fast, controlled and reached high conversions without the undesired side-reactions known for acrylamides. Dispersity decreased with time because of the high number of activation/deactivation cycles, in line with conventional ATRP. Induction periods were observed, and their duration increased as volume increased from 0.04, 1, 5, 10 to 15 L (from about 15 min to 3 h). Nevertheless, these induction periods are the compromise between reaction time, rate of O_2 consumption and instrumental limitations. Further optimizations should address this aspect, including improved mass transfer. The anodic dissolution of Al can be calculated from Faraday's laws of electrolysis. In H_2O, electrogenerated Al^{3+} did not pose any threat to the polymerization (< 0.43 g of Al were dissolved during the 15 L *se*ATRP). We also highlight the very low power consumption of these reactions: only at 15 L the peak power exceeded 1 W. The evolution of normalized molecular weight distributions is shown in Fig. 5.

Regardless of the reaction volume (0.04 L − 15 L), the chromatograms showed almost all monomodal, and almost symmetric molecular weight distributions, with no tailing, shifting to higher log$M$ as conversion increased. Fig. 6 shows how surface area and S/V (a), conversion and molecular weight (b) and $Đ$ (c) changed with the reaction volume. As V increased faster than S, the ratio S/V decreased. The best results in terms of conversion, polymer molecular weight and dispersity were obtained for higher S/V ratios (>0.4 cm^{-1}). When S/V was decreased, conversion and M_n decreased, while $Đ$ increased, all parameters stabilizing as S/V approached 0.2 cm^{-1}. Geometry plays a key role in every reactor design, and it is object of continuous extensive study and optimization [107–110]. Future design of bigger reactors for *se*ATRP should critically evaluate geometry and how to increase the S/V ratio, perhaps treating the surface to make it porous or add an additional stainless steel electrode with an appropriate mesh size.

Based on energy data, monomer input, and conversion recorded at 15 L and energy cost (0.1548 €/KWh), the first euro of energy required by *se*ATRP is spent after producing ~ 1912 kg of polyacrylamide. Most industries now already have a photovoltaic plant for energy self-production and, by using electricity from sunlight, *se*ATRP could theoretically enable polymer production with clean energy and limited additional cost. In addition, other equipment (computers, reactor heating/cooling system, analytical instruments), serving this scale-up plant,

Table 3
Effect of volume increase (scale-up) of *se*ATRP of AAm (10 wt%) at $T = 10$ °C.

Entry	Scale-up factor[b]	V (L)	Electrolyis program	t (h)	Conv.[c] (%)	$10^{-3} \times M_n^{GPC}$ [d]	$10^{-3} \times M_n^{th}$ [e]	$Đ$[f]	Q (C)	Peak power[g] (W)	Al dissolution (mg)[h]
1	2.6	0.04	I	2.5	93	40.3	46.8	1.24	8.17	< 0.01	0.76
2	33.3	0.5	II	2.5	97	42.9	48.6	1.16	78.74	0.04	7.39
3	66.6	1	II	3.5	97	46.5	48.6	1.17	245.60	0.27	22.91
4	333.3	5	IV	4.5	88	34.7	44.3	1.27	1527.60	0.43	142.43
5	666.6	10	V	6.0	79	40.7	40.0	1.27	3523.60	0.65	328.68
6	1000	15	VI	6.5	79	41.0	40.0	1.25	4596.70	1.01	428.77

[a]Conditions: [AAm]/[HEBiB]/[$CuBr_2$]/[Me_6TREN] = 703/1/0.5/2, where DP = 703 for AAm; $C_{Cu(II)} = 5 \times 10^{-4}$ M; $T = 10$ °C. WE = SS304 body of the reactor; CE = 750 cm aluminum coil directly immersed into the working solution. Stirring = 700 rpm. [b]Scale-up factor = Target volume/0.015 L. [c]Calculated from ^{1}H NMR in D_2O + 2 vol% DMF as internal standard. [d]Calculated from aqueous GPC with 6 narrow poly(sodium methacrylate) standards at $T = 35$ °C. [e]Calculated from ^{1}H NMR: M_n^{th} = Conv. × DP × MW_{AAm} + MW_{HEBiB}. [f]$Đ = M_w/M_n$. [g]The peak power is measured by the galvanostat during all the reaction time and the highest value recorded is reported. [h]Al anodic dissolution is calculated as $m_{Al} = Q/3F \times MW_{Al}$.

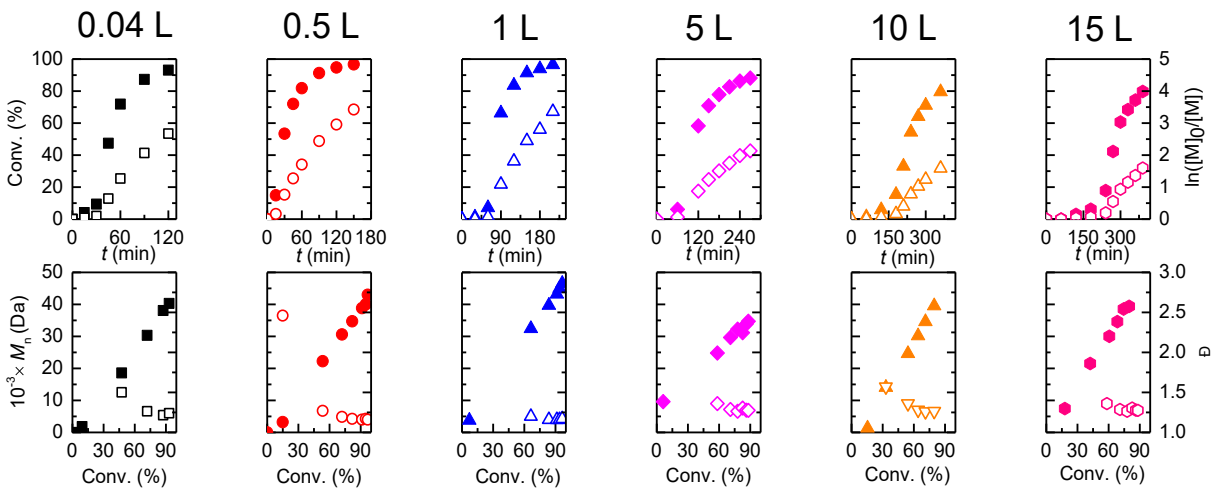

Fig. 4. Galvanostatic *se*ATRP of AAm from 0.04 to 15 L. First row: evolution of conversion (filled symbols) and ln([M]$_0$/[M]) (empty symbols) vs time; second row: evolution of M_n^{GPC} (filled symbols) and $Đ$ (empty symbols) vs conversion.

may also be powered by renewable energy.

2.4. Exploratory self-degassing seATRP of other monomers.

After the scaling-up, we also examined the self-degassing *se*ATRP of a selection of functional hydrophilic monomers such as oligo(ethylene oxide) methyl ether methacrylate ($OEOMA_{500}$), methacrylic acid (MAA), acrylic acid (AA), *N*-isopropylacrylamide (NIPAAm), *N*-hydroxyethylacrylamide (HEAAm) and methacrylamide (MAAm) in the 15 mL electrochemical cell (Table 4 **and Figures S14-S19**). These polymers are commonly used in various fields: OEOMA for bioconjugates/biocompatibility [16,111], acrylic and methacrylic acids for polyelectrolytes and pH-responsive (co)polymers [112,113], NIPAAm for thermoresponsive (co)polymers [111,114], and HEAAm for antibacterial and antifouling coatings [115]. The uncommon and undervalued MAAm could be used in thermoresponsive (co)polymers as well [116]. MAA and AA were polymerized by *e*ATRP at pH 1.0 and 2.0, respectively, as *se*ATRP does not strictly require a buffer [117]. This is advantageous in contrast to PICAR ATRP, which requires a very tight pH control due to photochemical side-reactions [12].

NIPAAm and HEAAm reached 99% conversion in ≤ 1 h producing well-controlled polymers, whereas $OEOMA_{500}$ reached moderate conversion with $[Cu^{II}TPMA]^{2+}$ (TPMA = tris(2-pyridylmethyl)amine), the usual catalyst for ATRP in H_2O [78,101]. Methacrylamide (MAAm) is one of the most challenging monomers for ATRP, to the best of our knowledge. While only few derivates of MAAm (such as hydroxypropyl methacrylamide and *N*-methyl methacrylamide) have been polymerized by ATRP or reversible addition-fragmentation chain-transfer (RAFT) polymerization, [118–120] controlled ATRP of unsubstituted MAAm has not been reported. MAAm has k_p of the same order as methacrylates [116,121], but k_{act} of the dormant P_n-X should be higher than that of acrylamide because of the tertiary nature of the terminal C-X. Moreover, PMAAm shows upper critical solution temperature (UCST) near 40 °C in H_2O [116]. ATRP of MAAm in H_2O must balance two conflicting requirements: 1) ensuring polymer solubility, and 2) suppressing intramolecular cyclization side-reactions. Both requirements are temperature-dependent: PMAAm is only soluble above 40 °C, but at this temperature cyclization is much more rapid than at 0–10 °C, consuming chain-ends during conversion [83,85,87,100]. We therefore attempted the *se*ATRP of MAAm just above its UCST to ensure full solubility, using 0.3 M NaCl to minimize intramolecular cyclization and $E_{app} = E_{1/2} + 0.06$ V to avoid excessive radical formation. The initiator was the polychlorinated hexafunctional hexachloro-2-propanone (HCA), which was also used for AAm (see **Section S5**). This is the first time that HCA is used as initiator in ATRP to the best of our knowledge. PMAAm-Cl was obtained with 47 % conversion and $Đ = 1.46$, but side reactions were only partially prevented, as judged by the incomplete conversion. For (M)AA, these are the first *se*ATRPs with a sacrificial aluminum anode. It is also worth noting that the reaction between electrogenerated H_2O_2 and pyruvic acid/pyruvic anion is strongly pH-dependent and is significantly attenuated at low pH [95]. In addition, pyruvate is present in the non-ionized pyruvic acid form at low pH. In view of this, we added pure pyruvic acid to the mixture. At 0.3 M of pyruvic acid, ROS scrubbing still occurred, and polymerizations were carried out up to moderate conversions, showing that a suitable concentration of pyruvic acid is effective at low pH. P(M)AA-Cl was

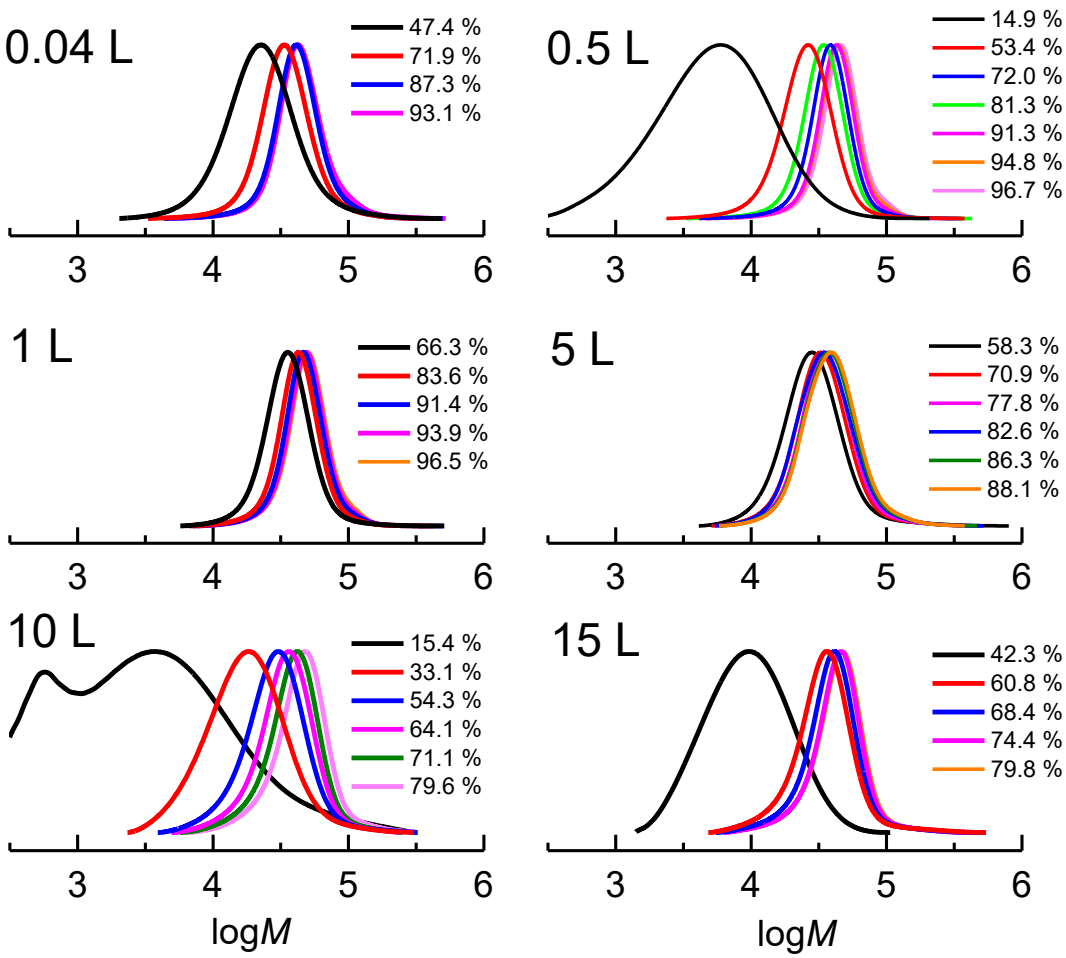

Fig. 5. Normalized evolution of molecular weight distribution of PAAm produced by galvanostatic *se*ATRP from 0.04 to 15 L. At 10 L, bimodality in the first chromatogram at conv. = 15.4% appeared because the signal of the polymer partially overlapped with the signal that corresponds to the eluent at the limit of the retention regime of our columns.

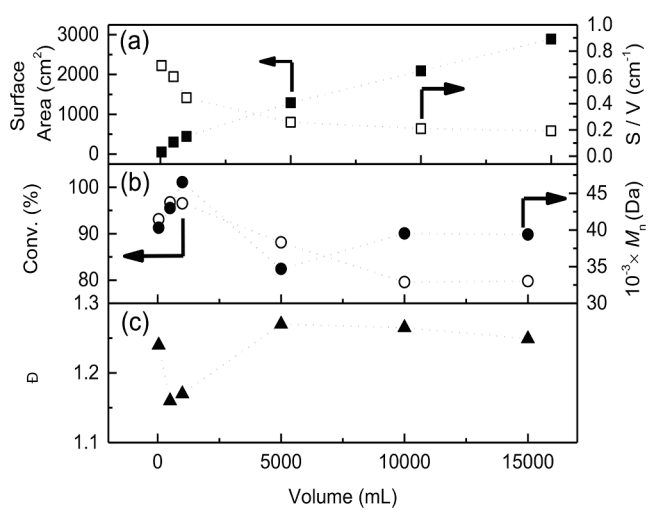

Fig. 6. Evolution of a) geometric surface area (■) and surface/volume ratio (□), b) conversion (●) and apparent molecular weight (○), and c) $Đ$ (▲) recorded at the end of *se*ATRP of AAm at 0.04, 0.5, 1, 5, 10 and 15 L.

obtained with low dispersity ($Đ < 1.3$). Evolution of normalized molecular weight distributions of water-soluble polymers produced by self-degassing potentiostatic *se*ATRP is shown in Fig. 7:

2.5. Chain extension of PAAm.

To prove the livingness of PAAm-Br, a chain extension was attempted. A short PAAm-Br macroinitiator was prepared by electrolyzing for 15 min a polymerization mixture prepared as of Table 1, **entry 5**. NMR and GPC analysis of this solution showed 11.4% AAm conv. (DP = 80), yielding PAAm-Br with M_n = 5900. 1 mL of this mixture containing PAAm-Br as macroinitiator was withdrawn. Then, the chain extension was continued by injecting this 1 mL of PAAm-Br mixture in a new mixture prepared as of Table 4, **entry 2**, with HEAAm as the second monomer. Electrolysis was triggered at $E_{app} = E_{pc}$. Considering the low AAm amount injected, competition between AAm and HEAAm during the synthesis of the second block was minimal. In addition, the reactivity ratio of AAm/HEAAm is close to 1 ($r_{AAm} \sim 1$, $r_{HEAAm} \sim 1$, and $r_{AAm} \times r_{HEAAm} \sim 1$) so that the majority of the second block should contain HEAAm and very few units of AAm statistically distributed along the chain [122]. The block copolymer, $PAAm_{88}$-*b*-$PHEAAm_{256}$-Br, had a $M_{n,}^{SEC} = 36.3 \times 10^3$, $M_{n,}^{th} = 35.4 \times 10^3$, $Đ = 1.30$ and conv.$_{HEAAm}$ = 53 %. MW distribution traces indicated extension and the peak shifted almost entirely towards higher MW (Fig. 8).

3. Conclusions

Controlled radical polymerizations by *se*ATRP in large volume reactors of up to 15 L were achieved by embedding an O_2 scavenging system in the *e*ATRP equilibrium. All reactions were powered by renewable energy taken from a photovoltaic system. The headspace was

Table 4
Potentiostatic self-degassing *se*ATRP of hydrophilic monomers (NIPAAm, and MAAm 10 wt% and HEAAm, $OEOMA_{500}$, MAA and AA 10 vol%) at a Pt cathode and a sacrificial Al anode, with pyruvic acid/pyruvate anion as ROS scrubber [a].

Entry	SE[b] (M)	Catalyst	E_{app}	Pyruvate (M)	t (h)	Conv.[c] (%)	$10^{-3} \times M_n^{GPC}$	$10^{-3} \times M_n^{th}$ [d]	$Đ$		pH	T (°C)
NIPAAm	0.1 NaBr	$[Cu^{II}Me_6TREN]^{2+}$	E_{pc}	0.05	1	99	53.1[e]	49.5	1.05	1.07	7.4	0
HEAAm	0.1 NaBr	$[Cu^{II}Me_6TREN]^{2+}$	E_{pc}	0.05	0.75	99	61.8[f]	61.4	1.30	2.28	7.4	0
MAAm	0.3 NaCl	$[Cu^{II}Me_6TREN]^{2+}$	$E_{1/2} + 0.06$	0.05	2	47	33.3[g]	23.6	1.46	4.13	7.4	42
$OEOMA_{500}$	0.1 NaCl	$[Cu^{II}TPMA]^{2+}$	$E_{1/2} + 0.06$	0.05	4	61	67.6 [h]	36.2	1.13	3.36	7.4	25
MAA	0.3 NaCl	$[Cu^{II}TPMA]^{2+}$	E_{pc}	0.3[i]	3	71	45.7[f]	36.1	1.23	2.03	1.0	25
AA	0.006 NaCl	$[Cu^{II}TPMA]^{2+}$	E_{pc}	0.3[i]	6	52	38.4[f]	27.3	1.25	3.23	2.0	25

[a]Conditions: [NIPAAm]/[HEBiB]/[$CuBr_2$]/[Me_6TREN] = 884/2/0.5/2, DP = 442; [HEAAm]/[HEBiB]/[$CuBr_2$]/[Me_6TREN] = 965/2/0.5/2, DP = 482; [MAAm]/[HCA]/[$CuCl_2$]/[Me_6TREN] = 118/0.2/0.05/0.2, DP = 588, HCA = hexachloroacetone; [$OEOMA_{500}$]/[HEBiB]/[$CuBr_2$]/[TPMA] = 216/2/1/2, DP = 108; [MAA]/[DCPA]/[$CuCl_2$]/[TPMA] = 118/0.2/0.1/0.4, DP = 590, DCPA = 2,2-dichloropropionic acid; [AA]/[TCAA]/[$CuCl_2$]/[TPMA] = 146/0.2/0.1/0.4, DP = 729, TCAA = trichloroacetic acid. [b]Supporting electrolyte. [c]Calculated from ^{1}H NMR in D_2O + 2 vol% DMF as internal standard. [d]Calculated from ^{1}H NMR; M_n^{th} = Conv. × DP × $MW_{monomer} + MW_{RX}$. [e]Calculated from DMF GPC with 6 narrow poly(methyl methacrylate) standards at T = 60 °C. [f]Calculated from aqueous GPC with 6 narrow poly (sodium methacrylate) standards at T = 35 °C. [g]Calculated from THF GPC with 6 narrow poly(styrene) standards at T = 30 °C. [h]Calculated from aqueous GPC with 6 narrow poly(sodium methacrylate) standards at T = 50 °C. [i]Pyruvic acid was used instead of sodium pyruvate. Other conditions: $C_{Cu(II)} = 10^{-3}$ M; WE = Pt mesh (approx. 6 cm^2); CE = 10 cm aluminum coil directly immersed into the working solution. Stirring = 700 rpm.

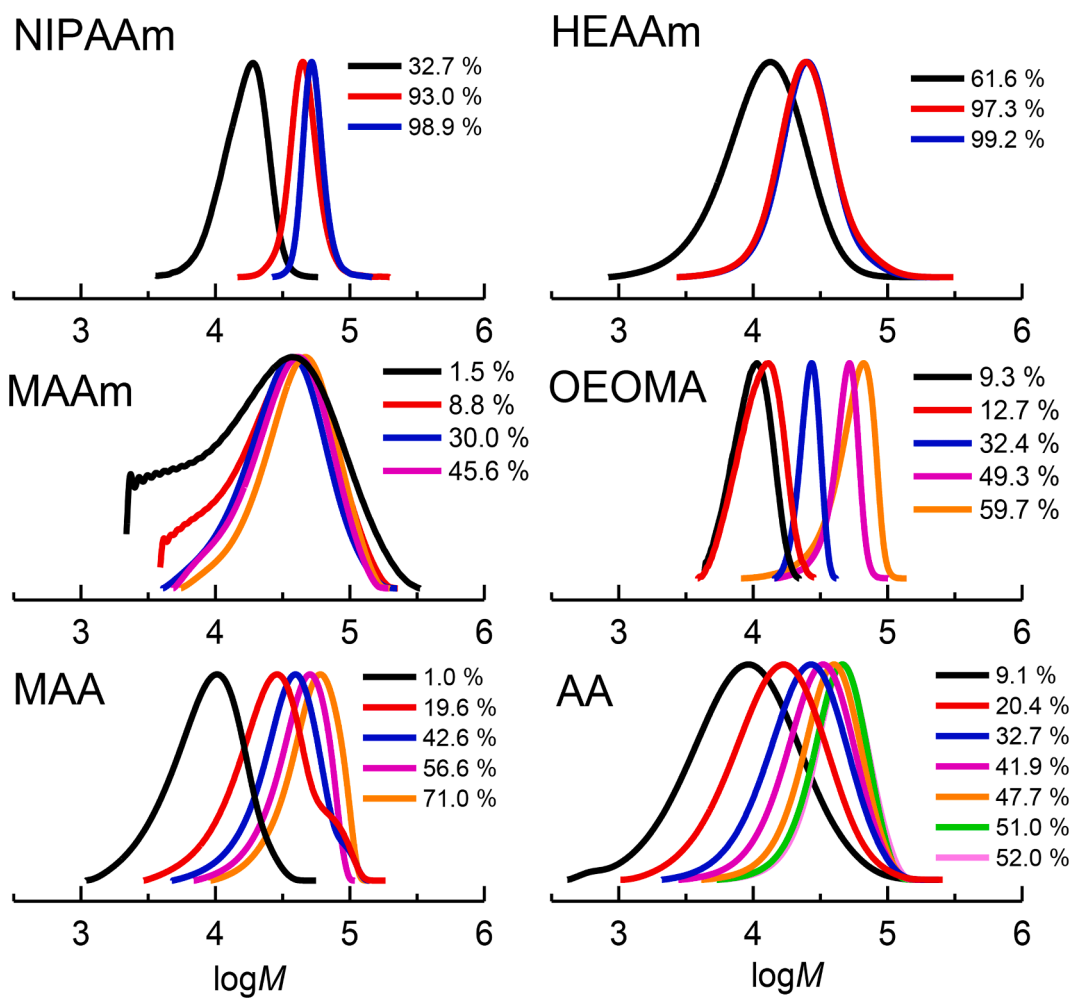

Fig. 7. Evolution of normalized molecular weight distributions of water-soluble polymers produced by self-degassing potentiostatic *se*ATRP at 15 mL at pH 7.4 (NIPAAm, HEAAm, MAAm and $OEOMA_{500}$), 2.0 (AA) and 1.0 (MAA).

degassed with N_2, while the presence of sodium pyruvate in solution ensured a relatively rapid self-degassing of the mixture once the electrolysis started. Sodium pyruvate reacts with ROS, preventing poisoning of the polymerization. Mechanistically, the process has some steps in common with PICAR ATRP [12], but the electrochemical control circumvents the radical generation that occurs during PICAR ATRP, allowing for decreasing the concentration of sodium pyruvate to 0.05 M to obtain an effective scrub. All AAm polymerizations from 15 mL to 15 L (scale-up factor 1000) were very well-controlled ($Đ$ < 1.27) and achieved high monomer conversions (>79%) in a relatively short time (<6.5 h). Moreover, pH control in *se*ATRP is not a strict requisite, in contrast to PICAR ATRP, because pH-changing side reactions occurring in the photochemical cycle do not occur in *se*ATRP. Thanks to this, we polymerized several other water-soluble monomers, including (meth)

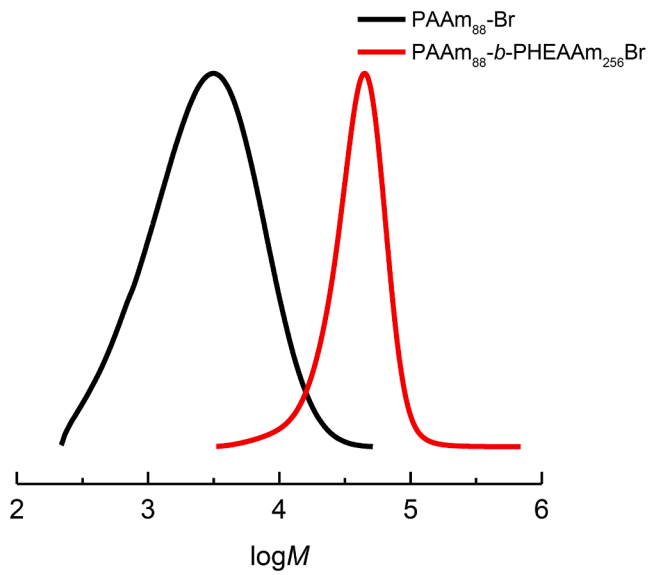

Fig. 8. Evolution of normalized molecular weight distributions of $PAAm_{80}$-Br and $PAAm_{80}$-*b*-$PHEAAm_{256}$-Br produced by self-degassing potentiostatic *se*ATRP in a 15 mL electrochemical cell.

acrylic acids (at pH $\leq$ 2), in the presence of sodium pyruvate or pyruvic acid, using either $[Cu^{II}Me_6TREN]^{2+}$ (for AAm, HEAAm, NIPAAm, MAAm) or $[Cu^{II}TPMA]^{2+}$ (for OEOMA, MAA, AA) as catalyst. The applicability of this process to hydrophobic monomers is currently under investigation in our laboratory and it will be reported in near future. However, the scale-up for hydrophobic monomers is hard to be achieved by homogeneous polymerizations, due to the cost of solvent and organic electrolytes, even by employing relatively inexpensive solvents like ethanol. A final issue is that sodium pyruvate is not soluble in organic solvents. *e*ATRP is currently a known and well-established technique for polymer synthesis, and its expansion to reactors with volumes $\geq$ 100 L is envisioned. Further challenges for *se*ATRP on an industrial scale may include: i) an improved electrode configuration for homogeneous electric field distribution, ii) the implementation of mechanical stirring for improved mass transfer, minimization of deoxygenation time, and online sensing elements for real-time reaction monitoring, and iii) expansion to non-homogeneous polymerizations.

CRediT authorship contribution statement

Francesco De Bon: Conceptualization, Investigation, Formal analysis, Writing – original draft, Writing – review & editing, Funding acquisition, Validation, Supervision. **Rita G. Fonseca:** Writing – review & editing, Validation. **Francesca Lorandi:** Investigation, Formal analysis, Writing – original draft, Writing – review & editing, Validation. **Arménio C. Serra:** Writing – review & editing, Validation. **Abdirisak A. Isse:** Writing – review & editing, Validation. **Krzysztof Matyjaszewski:** Writing – review & editing, Funding acquisition, Validation. **Jorge F.J. Coelho:** Conceptualization, Writing – review & editing, Funding acquisition, Validation, Supervision.

Declaration of Competing Interest

The authors declare that they have no known competing financial interests or personal relationships that could have appeared to influence the work reported in this paper.

Acknowledgments

The authors acknowledge Diana C. M. Ribeiro for her technical support during the synthesis of Me_6TREN and HEBiB, Dr. Kurt Olson for his comments during the manuscript preparation. F. De Bon thanks FCT for the project POCI-01-0145-FEDER-029742 (POLYCEL) and the project PTDC/EQU-EQU/2686/2020 (POLYELECTRON). Rita G. Fonseca thanks FCT for her PhD scholarship (SFRH/BD/133040/2017). Funding from MATIS (CENTRO-01-0145-FEDER-000014), co-financed by the European Regional Development Fund (FEDER) through "Programa Operacional Regional do Centro" (CENTRO2020) is also acknowledged. The NMR data were obtained at the Nuclear Magnetic Resonance Laboratory of the Coimbra Chemistry Centre (http://www.nmrccc.uc.pt), University of Coimbra, supported in part by Grant REEQ/481/QUI/2006 from FCT, POCI-2010, and FEDER, Portugal. This research was partially sponsored by FEDER funds through the program COMPETE – Programa Operacional Factores de Competitividade – and by national funds through FCT – Fundação para a Ciência e a Tecnologia, under the project UIDB/00285/2020. FL and KM acknowledge support from NSF (CHE 2000391).

Appendix A. Supplementary data

Supplementary data to this article can be found online at https://doi.org/10.1016/j.cej.2022.136690.

References

[1] M. Berton, J.M. de Souza, I. Abdiaj, D.T. McQuade, D.R. Snead, Scaling continuous API synthesis from milligram to kilogram: extending the enabling benefits of micro to the plant, J. Flow Chem. 10 (2020) 73–92.
[2] T. Noël, Y. Cao, G. Laudadio, The fundamentals behind the use of flow reactors in electrochemistry, Acc. Chem. Res. 52 (10) (2019) 2858–2869.
[3] A.E. Enciso, F. Lorandi, A. Mehmood, M. Fantin, G. Szczepaniak, B.G. Janesko, K. Matyjaszewski, p-Substituted Tris(2-pyridylmethyl)amines as ligands for highly active ATRP catalysts: facile synthesis and characterization, Angew. Chem. Int. Ed. Engl. 59 (35) (2020) 14910–14920.
[4] T.G. Ribelli, F. Lorandi, M. Fantin, K. Matyjaszewski, Atom transfer radical polymerization: billion times more active catalysts and new initiation systems, Macromol. Rapid Commun. 40 (2019), e1800616.
[5] L.B. Levy, Inhibitor-oxygen interactions in acrylic acid stabilization, Plant/Operations Progress 6 (4) (1987) 188–189.
[6] R. Li, F.J. Schork, Modeling of the inhibition mechanism of acrylic acid polymerization, Ind. Eng. Chem. Res. 45 (9) (2006) 3001–3008.
[7] S.C. Ligon, B. Husár, H. Wutzel, R. Holman, R. Liska, Strategies to reduce oxygen inhibition in photoinduced polymerization, Chem. Rev. 114 (1) (2014) 557–589.
[8] R. Simič, J. Mandal, K. Zhang, N.D. Spencer, Oxygen inhibition of free-radical polymerization is the dominant mechanism behind the "mold effect" on hydrogels, Soft Matter 17 (26) (2021) 6394–6403.
[9] B. Husár, S.C. Ligon, H. Wutzel, H. Hoffmann, R. Liska, The formulator's guide to anti-oxygen inhibition additives, Prog. Org. Coat. 77 (11) (2014) 1789–1798.
[10] F. Tudos, T. Foldesberezsnich, Free-radical polymerization: Inhibition and retardation, Prog. Polym. Sci. 14 (6) (1989) 717–761.
[11] M. Langerman, D.G.H. Hetterscheid, Fast oxygen reduction catalyzed by a copper (II) Tris(2-pyridylmethyl)amine complex through a stepwise mechanism, Angew. Chem. Int. Ed. Engl. 58 (37) (2019) 12974–12978.
[12] G. Szczepaniak, M. Łagodzińska, S. Dadashi-Silab, A. Gorczyński, K. Matyjaszewski, Fully oxygen-tolerant atom transfer radical polymerization triggered by sodium pyruvate, Chem. Sci. 11 (33) (2020) 8809–8816.
[13] G. Szczepaniak, L. Fu, H. Jafari, K. Kapil, K. Matyjaszewski, Making ATRP more practical: oxygen tolerance, Acc. Chem. Res. 54 (7) (2021) 1779–1790.
[14] B. Maillard, K.U. Ingold, J.C. Scaiano, Rate constants for the reactions of free radicals with oxygen in solution, J. Am. Chem. Soc. 105 (15) (1983) 5095–5099.
[15] A. Marchaj, D.G. Kelley, A. Bakac, J.H. Espenson, Kinetics of the reactions between alkyl radicals and molecular oxygen in aqueous solution, The Journal of Physical Chemistry 95 (11) (1991) 4440–4441.
[16] S.L. Baker, B. Kaupbayeva, S. Lathwal, S.R. Das, A.J. Russell, K. Matyjaszewski, Atom transfer radical polymerization for biorelated hybrid materials, Biomacromolecules 20 (12) (2019) 4272–4298.
[17] M.S. Messina, K.M.M. Messina, A. Bhattacharya, H.R. Montgomery, H. D. Maynard, Preparation of biomolecule-polymer conjugates by grafting-from using ATRP, RAFT, or ROMP, Prog. Polym. Sci. 100 (2020), 101186.
[18] K. Matyjaszewski, S. Coca, S.G. Gaynor, M. Wei, B.E. Woodworth, Controlled radical polymerization in the presence of oxygen, Macromolecules 31 (17) (1998) 5967–5969.
[19] D. Konkolewicz, Y. Wang, P. Krys, M. Zhong, A.A. Isse, A. Gennaro, K. Matyjaszewski, SARA ATRP or SET-LRP. End of controversy?, Polymer Chemistry 5 (2014) 4409.
[20] D. Konkolewicz, Y.u. Wang, M. Zhong, P. Krys, A.A. Isse, A. Gennaro, K. Matyjaszewski, Reversible-deactivation radical polymerization in the presence of metallic copper, A Critical Assessment of the SARA ATRP and SET-LRP Mechanisms, Macromolecules 46 (22) (2013) 8749–8772.

[21] E. Liarou, R. Whitfield, A. Anastasaki, N.G. Engelis, G.R. Jones, K. Velonia, D. M. Haddleton, Copper-mediated polymerization without external deoxygenation or oxygen scavengers, Angew. Chem. Int. Ed. Engl. 57 (29) (2018) 8998–9002.
[22] T. Zhang, E.M. Benetti, R. Jordan, Surface-initiated Cu(0)-mediated CRP for the rapid and controlled synthesis of quasi-3D structured polymer brushes, ACS Macro Lett. 8 (2) (2019) 145–153.
[23] T. Zhang, Y. Du, J. Kalbacova, R. Schubel, R.D. Rodriguez, T. Chen, D.R.T. Zahn, R. Jordan, Wafer-scale synthesis of defined polymer brushes under ambient conditions, Polym. Chem. 6 (47) (2015) 8176–8183.
[24] Y. Che, T. Zhang, Y. Du, I. Amin, C. Marschelke, R. Jordan, "On Water" surface-initiated polymerization of hydrophobic monomers, Angew. Chem. Int. Ed. Engl. 57 (50) (2018) 16380–16384.
[25] W. Yan, M. Fantin, S. Ramakrishna, N.D. Spencer, K. Matyjaszewski, E.M. Benetti, Growing polymer brushes from a variety of substrates under ambient conditions by Cu(0)-mediated surface-initiated ATRP, ACS Appl Mater Interfaces 11 (30) (2019) 27470–27477.
[26] W. Yan, M. Fantin, N.D. Spencer, K. Matyjaszewski, E.M. Benetti, Translating surface-initiated atom transfer radical polymerization into technology: the mechanism of Cu0-mediated SI-ATRP under environmental conditions, ACS Macro Lett. 8 (2019) 865–870.
[27] A.S.R. Oliveira, P.V. Mendonça, A.C. Serra, J.F.J. Coelho, Self-degassing SARA ATRP mediated by $Na_2S_2O_4$ with no external additives, Journal of Polymer Science 58 (1) (2020) 145–153.
[28] M. Rolland, N.P. Truong, R. Whitfield, A. Anastasaki, Tailoring polymer dispersity in photoinduced iron-catalyzed ATRP, ACS Macro Lett. 9 (4) (2020) 459–463.
[29] A. Layadi, B. Kessel, W. Yan, M. Romio, N.D. Spencer, M. Zenobi-Wong, K. Matyjaszewski, E.M. Benetti, Oxygen tolerant and cytocompatible iron(0)-mediated ATRP enables the controlled growth of polymer brushes from mammalian cell cultures, J. Am. Chem. Soc. 142 (6) (2020) 3158–3164.
[30] M.R. Bennett, P. Gurnani, P.J. Hill, C. Alexander, F.J. Rawson, Iron-catalysed radical polymerisation by living bacteria, Angew. Chem. Int. Ed. Engl. 59 (12) (2020) 4750–4755.
[31] M. Słowikowska, K. Chajec, A. Michalski, S. Zapotoczny, K. Wolski, Surface-initiated photoinduced iron-catalyzed atom transfer radical polymerization with ppm concentration of FeBr 3 under visible light, Materials 13 (2020) 5139.
[32] R. Faggion Albers, W. Yan, M. Romio, E.R. Leite, N.D. Spencer, K. Matyjaszewski, E.M. Benetti, Mechanism and application of surface-initiated ATRP in the presence of a Zn0 plate, Polym. Chem. 11 (44) (2020) 7009–7014.
[33] A. Simakova, S.E. Averick, D. Konkolewicz, K. Matyjaszewski, Aqueous ARGET ATRP, Macromolecules 45 (16) (2012) 6371–6379.
[34] K.e. Min, H. Gao, K. Matyjaszewski, Use of ascorbic acid as reducing agent for synthesis of well-defined polymers by ARGET ATRP, Macromolecules 40 (6) (2007) 1789–1791.
[35] W. Jakubowski, K.e. Min, K. Matyjaszewski, Activators regenerated by electron transfer for atom transfer radical polymerization of styrene, Macromolecules 39 (1) (2006) 39–45.
[36] H. Dong, K. Matyjaszewski, ARGET ATRP of 2-(Dimethylamino)ethyl methacrylate as an intrinsic reducing agent, Macromolecules 41 (19) (2008) 6868–6870.
[37] A.E. Enciso, L. Fu, A.J. Russell, K. Matyjaszewski, A breathing atom-transfer radical polymerization: fully oxygen-tolerant polymerization inspired by aerobic respiration of cells, Angew. Chem. Int. Ed. 57 (2018) 933–936.
[38] A.E. Enciso, L. Fu, S. Lathwal, M. Olszewski, Z. Wang, S.R. Das, A.J. Russell, K. Matyjaszewski, Biocatalytic "oxygen-fueled" atom transfer radical polymerization, Angew. Chem. Int. Ed. Engl. 57 (49) (2018) 16157–16161.
[39] G. Zain, D. Bondarev, J. Doháňošová, J. Mosnáček, Oxygen-tolerant photochemically induced atom transfer radical polymerization of the renewable monomer tulipalin A, Chemphotochem 3 (11) (2019) 1138–1145.
[40] J. Mosnáček, A. Eckstein-Andicsová, K. Borská, Ligand effect and oxygen tolerance studies in photochemically induced copper mediated reversible deactivation radical polymerization of methyl methacrylate in dimethyl sulfoxide, Polym. Chem. 6 (13) (2015) 2523–2530.
[41] G. Fan, A.J. Graham, J. Kolli, N.A. Lynd, B.K. Keitz, Aerobic radical polymerization mediated by microbial metabolism, Nat Chem 12 (7) (2020) 638–646.
[42] J. Yeow, R. Chapman, A.J. Gormley, C. Boyer, Up in the air: oxygen tolerance in controlled/living radical polymerisation, Chem. Soc. Rev. 47 (2018) 4357–4387.
[43] K. Borska, D. Moravcikova, J. Mosnacek, Photochemically induced ATRP of (Meth)acrylates in the presence of air: the effect of light intensity, ligand, and oxygen concentration, Macromol. Rapid Commun. 38 (2017) 1600639.
[44] Q. Yang, J. Lalevée, J. Poly, Development of a robust photocatalyzed ATRP mechanism exhibiting good tolerance to oxygen and inhibitors, Macromolecules 49 (20) (2016) 7653–7666.
[45] M. Rolland, R. Whitfield, D. Messmer, K. Parkatzidis, N.P. Truong, A. Anastasaki, Effect of polymerization components on oxygen-tolerant photo-ATRP, ACS Macro Lett. 8 (12) (2019) 1546–1551.
[46] J.-K. Guo, Y.-N. Zhou, Z.-H. Luo, Electrochemically mediated ATRP process intensified by ionic liquid: A "flash" polymerization of methyl acrylate, Chem. Eng. J. 372 (2019) 163–170.
[47] J.-K. Guo, Y.-N. Zhou, Z.-H. Luo, Iron-based electrochemically mediated atom transfer radical polymerization with tunable catalytic activity, AlChE J. 64 (3) (2018) 961–969.
[48] J.-K. Guo, Y.-N. Zhou, Z.-H. Luo, Kinetic insights into the iron-based electrochemically mediated atom transfer radical polymerization of methyl methacrylate, Macromolecules 49 (11) (2016) 4038–4046.
[49] Y. Wang, C. Bian, W. Feng, N. Yang, Ultrasonication enhanced photocatalytic solvent-free reversible deactivation radical polymerization up to high conversion with good control, Eur. Polym. J. 168 (2022), 111118.
[50] C. Bian, Y.-N. Zhou, J.-K. Guo, Z.-H. Luo, Photoinduced Fe-mediated atom transfer radical polymerization in aqueous media, Polym. Chem. 8 (47) (2017) 7360–7368.
[51] G.J. Dunderdale, C. Urata, D.F. Miranda, A. Hozumi, Large-scale and environmentally friendly synthesis of pH-responsive oil-repellent polymer brush surfaces under ambient conditions, ACS Appl Mater Interfaces 6 (15) (2014) 11864–11868.
[52] P. Pavan, F. Lorandi, F. De Bon, A. Gennaro, A.A. Isse, Enhancement of the rate of atom transfer radical polymerization in organic solvents by addition of water: an electrochemical study, Chemelectrochem 8 (2021) 2450–2458.
[53] D. Bondarev, K. Borska, M. Soral, D. Moravcikova, J. Mosnacek, Simple tertiary amines as promotors in oxygen tolerant photochemically induced ATRP of acrylates, Polymer 161 (2019) 122–127.
[54] A. Theodorou, P. Mandriotis, A. Anastasaki, K. Velonia, Oxygen tolerant, photoinduced controlled radical polymerization approach for the synthesis of giant amphiphiles, Polym. Chem. 12 (15) (2021) 2228–2235.
[55] N. Li, X.C. Pan, Controlled radical polymerization: from oxygen inhibition and tolerance to oxygen initiation, Chin. J. Polym. Sci. 39 (2021) 1084–1092.
[56] L. Quirós-Montes, G.A. Carriedo, J. García-Álvarez, A. Presa Soto, Deep eutectic solvents for Cu-catalysed ARGET ATRP under an air atmosphere: a sustainable and efficient route to poly(methyl methacrylate) using a recyclable Cu(ii) metal–organic framework, Green Chem. 21 (2019) 5865–5875.
[57] A.J.D. Magenau, N.C. Strandwitz, A. Gennaro, K. Matyjaszewski, Electrochemically mediated atom transfer radical polymerization, Science 332 (6025) (2011) 81–84.
[58] P. Chmielarz, M. Fantin, S. Park, A.A. Isse, A. Gennaro, A.J.D. Magenau, A. Sobkowiak, K. Matyjaszewski, Electrochemically mediated atom transfer radical polymerization (eATRP), Prog. Polym. Sci. 69 (2017) 47–78.
[59] H. Sun, J. Kong, Q. Wang, Q. Liu, X. Zhang, Dual signal amplification by eATRP and DNA-templated silver nanoparticles for ultrasensitive electrochemical detection of nucleic acids, ACS Appl Mater Interfaces 11 (31) (2019) 27568–27573.
[60] B. Zhao, M. Mohammed, B. A. Jones, P. Wilson, Plug-and-play aqueous electrochemical atom transfer radical polymerization, Chem Commun (Camb) 57 (32) (2021) 3897–3900.
[61] A.A. Isse, A. Gennaro, Electrochemistry for atom transfer radical polymerization, Chem Rec 21 (9) (2021) 2203–2222.
[62] A.J.D. Magenau, N. Bortolamei, E. Frick, S. Park, A. Gennaro, K. Matyjaszewski, Investigation of electrochemically mediated atom transfer radical polymerization, Macromolecules 46 (11) (2013) 4346–4353.
[63] B. Li, B.o. Yu, W.T.S. Huck, F. Zhou, W. Liu, Electrochemically induced surface-initiated atom-transfer radical polymerization, Angew. Chem. Int. Ed. Engl. 51 (21) (2012) 5092–5095.
[64] S. Park, P. Chmielarz, A. Gennaro, K. Matyjaszewski, Simplified electrochemically mediated atom transfer radical polymerization using a sacrificial anode, Angew. Chem. Int. Ed. 54 (8) (2015) 2388–2392.
[65] F. De Bon, A.A. Isse, A. Gennaro, Towards scale-up of electrochemically-mediated atom transfer radical polymerization: Use of a stainless-steel reactor as both cathode and reaction vessel, Electrochim. Acta 304 (2019) 505–512.
[66] F. Lorandi, M. Fantin, A.A. Isse, A. Gennaro, Electrochemically mediated atom transfer radical polymerization of n-butyl acrylate on non-platinum cathodes, Polym. Chem. 7 (34) (2016) 5357–5365.
[67] M. Fantin, F. Lorandi, A.A. Isse, A. Gennaro, Sustainable electrochemically-mediated atom transfer radical polymerization with inexpensive non-platinum electrodes, Macromol. Rapid Commun. 37 (16) (2016) 1318–1322.
[68] N. Hadjichristidis, H. Iatrou, S. Pispas, M. Pitsikalis, Anionic polymerization: high vacuum techniques, J Polym Sci Pol Chem 38 (18) (2000) 3211–3234.
[69] D. Uhrig, J.W. Mays, Experimental techniques in high-vacuum anionic polymerization, J Polym Sci Pol Chem 43 (24) (2005) 6179–6222.
[70] M. Lynch, Manufacture and use of chloroprene monomer, Chem. Biol. Interact. 135 (2001) 155–167.
[71] S.C. Perry, C. Ponce de León, F.C. Walsh, Review—the design, performance and continuing development of electrochemical reactors for clean electrosynthesis, J. Electrochem. Soc. 167 (2020), 155525.
[72] T. Tzedakis, A. Savall, Performance predictions in the scale-up of a liquid—liquid CSTR for indirect electro-oxidation of aromatic hydrocarbons, Chem. Eng. Sci. 46 (9) (1991) 2269–2279.
[73] S. Shanmugam, K. Matyjaszewski, Reversible deactivation radical polymerization: state-of-the-art in 2017, reversible deactivation radical polymerization: mechanisms and synthetic methodologies, American Chemical Society 2018 (2017) 1–39.
[74] X. Pan, M. Fantin, F. Yuan, K. Matyjaszewski, Externally controlled atom transfer radical polymerization, Chem. Soc. Rev. 47 (14) (2018) 5457–5490.
[75] T.F.C.V. Silva, A. Fonseca, I. Saraiva, R.A.R. Boaventura, V.J.P. Vilar, Scale-up and cost analysis of a photo-Fenton system for sanitary landfill leachate treatment, Chem. Eng. J. 283 (2016) 76–88.
[76] F.A. Ferrari, J.F.B. Pereira, G.-J. Witkamp, M.B.S. Forte, Which Variables matter for process design and scale-up? A Study of Sugar Cane Straw Pretreatment Using Low-Cost and Easily Synthesizable Ionic Liquids, ACS Sustainable Chemistry & Engineering 7 (15) (2019) 12779–12788.
[77] N. Bortolamei, A.A. Isse, A.J.D. Magenau, A. Gennaro, K. Matyjaszewski, Controlled aqueous atom transfer radical polymerization with electrochemical generation of the active catalyst, Angew. Chem. 123 (48) (2011) 11593–11596.

[78] M. Fantin, A.A. Isse, A. Gennaro, K. Matyjaszewski, Understanding the fundamentals of aqueous ATRP and defining conditions for better control, Macromolecules 48 (19) (2015) 6862–6875.
[79] W.A. Braunecker, N.V. Tsarevsky, A. Gennaro, K. Matyjaszewski, Thermodynamic components of the atom transfer radical polymerization equilibrium: quantifying solvent effects, Macromolecules 42 (2009) 6348–6360.
[80] P. Chmielarz, A. Sobkowiak, K. Matyjaszewski, A simplified electrochemically mediated ATRP synthesis of PEO-*b*-PMMA copolymers, Polymer 77 (2015) 266–271.
[81] P. Chmielarz, S. Park, A. Simakova, K. Matyjaszewski, Electrochemically mediated ATRP of acrylamides in water, Polymer 60 (2015) 302–307.
[82] P. Chmielarz, P. Krys, S. Park, K. Matyjaszewski, PEO-*b*-PNIPAM copolymers via SARA ATRP and eATRP in aqueous media, Polymer 71 (2015) 143–147.
[83] F. De Bon, S. Marenzi, A.A. Isse, C. Durante, A. Gennaro, Electrochemically mediated aqueous atom transfer radical polymerization of N N-Dimethylacrylamide, ChemElectroChem 7 (6) (2020) 1378–1388.
[84] R.W. Lewis, R.A. Evans, N. Malic, K. Saito, N.R. Cameron, Ultra-fast aqueous polymerisation of acrylamides by high power visible light direct photoactivation RAFT polymerisation, Polym. Chem. 9 (1) (2018) 60–68.
[85] G.R. Jones, Z. Li, A. Anastasaki, D.J. Lloyd, P. Wilson, Q. Zhang, D.M. Haddleton, Rapid synthesis of well-defined polyacrylamide by aqueous Cu(0)-mediated Reversible-Deactivation Radical Polymerization, Macromolecules 49 (2) (2016) 483–489.
[86] Y. Sun, H. Du, Y.i. Deng, Y. Lan, C. Feng, Preparation of polyacrylamide via surface-initiated electrochemical-mediated atom transfer radical polymerization (SI-eATRP) for Pb2+ sensing, J. Solid State Electrochem. 20 (1) (2016) 105–113.
[87] F. Alsubaie, A. Anastasaki, P. Wilson, D.M. Haddleton, Sequence-controlled multi-block copolymerization of acrylamides via aqueous SET-LRP at 0 °C, Polym. Chem. 6 (3) (2015) 406–417.
[88] D.A.Z. Wever, P. Raffa, F. Picchioni, A.A. Broekhuis, Acrylamide homopolymers and acrylamide–N-isopropylacrylamide block copolymers by atomic transfer radical polymerization in water, Macromolecules 45 (10) (2012) 4040–4045.
[89] N.H. Nguyen, B.M. Rosen, V. Percec, SET-LRP ofN,N-dimethylacrylamide and of N-isopropylacrylamide at 25 °C in protic and in dipolar aprotic solvents, J. Polym. Sci., Part A: Polym. Chem. 48 (2010) 1752-1763.
[90] P.-E. Millard, N.C. Mougin, A. Böker, A.H.E. Müller, Controlling the fast ATRP of N-isopropylacrylamide in water, controlled/living radical polymerization: progress in ATRP, American Chemical Society (2009) 127–137.
[91] W.v.B. Robertson, The preparation of sodium pyruvate, Science 96 (2482) (1942) 93–94.
[92] D. Grosjean, Atmospheric reactions of pyruvic acid, Atmos. Environ. 17 (1983) (1967) 2379–2382.
[93] E.C. Griffith, B.K. Carpenter, R.K. Shoemaker, V. Vaida, Photochemistry of aqueous pyruvic acid, Proc Natl Acad Sci USA 110 (29) (2013) 11714–11719.
[94] A.E. Reed Harris, B. Ervens, R.K. Shoemaker, J.A. Kroll, R.J. Rapf, E.C. Griffith, A. Monod, V. Vaida, Photochemical kinetics of pyruvic acid in aqueous solution, J. Phys. Chem. A 118 (37) (2014) 8505–8516.
[95] A. Lopalco, G. Dalwadi, S. Niu, R.L. Schowen, J. Douglas, V.J. Stella, Mechanism of decarboxylation of pyruvic acid in the presence of hydrogen peroxide, J. Pharm. Sci. 105 (2) (2016) 705–713.
[96] A.E. Reed Harris, A. Pajunoja, M. Cazaunau, A. Gratien, E. Pangui, A. Monod, E. C. Griffith, A. Virtanen, J.-F. Doussin, V. Vaida, Multiphase photochemistry of pyruvic acid under atmospheric conditions, J. Phys. Chem. A 121 (18) (2017) 3327–3339.
[97] F. De Bon, D.C.M. Ribeiro, C.M.R. Abreu, R.A.C. Rebelo, A.A. Isse, A.C. Serra, A. Gennaro, K. Matyjaszewski, J.F.J. Coelho, Under pressure: electrochemically-mediated atom transfer radical polymerization of vinyl chloride, Polym. Chem. 11 (2020) 6745–6762.
[98] M. Fantin, P. Chmielarz, Y.i. Wang, F. Lorandi, A.A. Isse, A. Gennaro, K. Matyjaszewski, Harnessing the interaction between surfactant and hydrophilic catalyst to control eATRP in miniemulsion, Macromolecules 50 (9) (2017) 3726–3732.
[99] V.G. Debabov, A.S. Yanenko, Biocatalytic hydrolysis of nitriles, Review, J. Chem. 1 (4) (2011) 385–402.
[100] A. Herberg, X. Yu, D. Kuckling, End group stability of atom transfer radical polymerization (ATRP)-synthesized Poly(N-isopropylacrylamide): perspectives for diblock copolymer synthesis, Polymers (Basel) 11 (2019) 678.
[101] M. Fantin, A.A. Isse, K. Matyjaszewski, A. Gennaro, ATRP in water: kinetic analysis of active and super-active catalysts for enhanced polymerization control, Macromolecules 50 (2017) 2696–2705.
[102] M. Fantin, A.A. Isse, N. Bortolamei, K. Matyjaszewski, A. Gennaro, Electrochemical approaches to the determination of rate constants for the activation step in atom transfer radical polymerization, Electrochim. Acta 222 (2016) 393–401.
[103] F. Lorandi, M. Fantin, A.A. Isse, A. Gennaro, K. Matyjaszewski, New protocol to determine the equilibrium constant of atom transfer radical polymerization, Electrochim. Acta 260 (2018) 648–655.
[104] F. Lorandi, K. Matyjaszewski, Why do we need more active ATRP catalysts? Isr. J. Chem. 60 (1-2) (2020) 108–123.
[105] E. Ntagia, E. Fiset, L. Truong Cong Hong, E. Vaiopoulou, K. Rabaey, Electrochemical treatment of industrial sulfidic spent caustic streams for sulfide removal and caustic recovery, J. Hazard. Mater. 388 (2020) 121770.
[106] M. Panizza, G. Cerisola, Electrochemical oxidation as a final treatment of synthetic tannery wastewater, Environ. Sci. Technol. 38 (20) (2004) 5470–5475.
[107] S. Bebelis, K. Bouzek, A. Cornell, M.G.S. Ferreira, G.H. Kelsall, F. Lapicque, C. Ponce de León, M.A. Rodrigo, F.C. Walsh, Highlights during the development of electrochemical engineering, Chem. Eng. Res. Des. 91 (10) (2013) 1998–2020.
[108] S. Gu, B. Xu, Y. Yan, Electrochemical energy engineering: a new frontier of chemical engineering innovation, Annu Rev Chem Biomol Eng 5 (1) (2014) 429–454.
[109] G.G. Botte, Electrochemical manufacturing in the chemical industry, Interface magazine 23 (3) (2014) 49–55.
[110] E. Mousset, C. Trellu, H. Olvera-Vargas, Y. Pechaud, F. Fourcade, M.A. Oturan, Electrochemical technologies coupled with biological treatments, Curr. Opin. Electrochem. 26 (2021), 100668.
[111] B. Kaupbayeva, A.J. Russell, Polymer-enhanced biomacromolecules, Prog. Polym. Sci. 101 (2020) 101194.
[112] Z. Qu, H. Xu, H. Gu, Synthesis and biomedical applications of poly((meth)acrylic acid) brushes, ACS Appl Mater Interfaces 7 (27) (2015) 14537–14551.
[113] A.E. Marras, J.M. Ting, K.C. Stevens, M.V. Tirrell, Advances in the structural design of polyelectrolyte complex micelles, J. Phys. Chem. B 125 (26) (2021) 7076–7089.
[114] L. Tang, L. Wang, X. Yang, Y. Feng, Y.u. Li, W. Feng, Poly(N-isopropylacrylamide)-based smart hydrogels: design, properties and applications, Prog. Mater Sci. 115 (2021) 100702.
[115] S. Lowe, N.M. O'Brien-Simpson, L.A. Connal, Antibiofouling polymer interfaces: poly(ethylene glycol) and other promising candidates, Polym. Chem. 6 (2015) 198–212.
[116] T. Eckert, V. Abetz, Polymethacrylamide—An underrated and easily accessible upper critical solution temperature polymer: Green synthesis via photoiniferter reversible addition–fragmentation chain transfer polymerization and analysis of solution behavior in water/ethanol mixtures, Journal of Polymer Science 58 (2020) 3050–3060.
[117] F. Lorandi, M. Fantin, Y. Wang, A.A. Isse, A. Gennaro, K. Matyjaszewski, Atom transfer radical polymerization of acrylic and methacrylic acids: preparation of acidic polymers with various architectures, ACS Macro Lett. 9 (2020) 693–699.
[118] N.H. Nguyen, C. Rodriguez-Emmenegger, E. Brynda, Z. Sedlakova, V. Percec, SET-LRP of N-(2-hydroxypropyl)methacrylamide in H_2O, Polym. Chem. 4 (2013) 2424.
[119] Y.A. Vasilieva, C.W. Scales, D.B. Thomas, R.G. Ezell, A.B. Lowe, N. Ayres, C. L. McCormick, Controlled/living polymerization of methacrylamide in aqueous media via the RAFT process, J. Polym. Sci., Part A: Polym. Chem. 43 (14) (2005) 3141–3152.
[120] Č. Koňák, B. Ganchev, M. Teodorescu, K. Matyjaszewski, P. Kopečková, J. Kopeček, Poly[N-(2-hydroxypropyl)methacrylamide-block-n-butyl acrylate] micelles in water/DMF mixed solvents, Polymer 43 (13) (2002) 3735–3741.
[121] J. Schrooten, I. Lacík, M. Stach, P. Hesse, M. Buback, Propagation kinetics of the radical polymerization of methylated acrylamides in aqueous solution, Macromol. Chem. Phys. 214 (20) (2013) 2283–2294.
[122] P.S. Mumick, C.L. McCormick, Water soluble copolymers. 54: *N*-isopropylacrylamide-co-acrylamide copolymers in drag reduction: Synthesis, characterization, and dilute solution behavior, Polym. Eng. Sci. 34 (1994) 1419–1428.